Rich Device Physics Found in Photoresponses of Low-Dimensional Photodetectors by Fitting With Explicit Photogain Theory

Kai Li, Jiajing He, Wenyu Zhang, Huayou Liu, and Yaping Dan, *Senior Member, IEEE*

Abstract—In this work, we employed our newly established explicit photogain theory to probe physics in nanodevices at single device level. A single fitting of the explicit photogain theory to experimental photoresponses allows us to find important device parameters including surface depletion region width W_{dep}, doping concentration N_A (or N_D), carrier mobility μ_p (or μ_n), minority recombination lifetime τ_0 and surface recombination velocity V_{srv}. These parameters are often difficult to calibrate using traditional semiconductor characterization techniques as the size of semiconductor devices scales down. The extracted parameters were verified with independent Hall effect measurements and other experiments. It shows that this technique is simple, nondestructive and accurate enough to probe the physics in nanodevices at single device level.

Index Terms—Silicon nanowire, photoresponse, doping concentration, carrier mobility, minority carrier life time, depletion region.

I. INTRODUCTION

THE size down-scaling of semiconductor devices significantly reduces the interaction of semiconductors at single device level with electric, magnetic and electromagnetic fields [1]–[6]. It thus becomes increasingly difficult to characterize the ultra-scaled semiconductor devices using these fields as a probe. For example, nanodevices often have tiny capacitances, which makes it extremely difficult, if not impossible, to probe defects at single device level using deep level transient spectroscopy (DLTS) [7]–[11], a well-stablished classical technique that detects the capacitance variation by charging or discharging defect states in semiconductors. It is thus important and valuable to develop a technology that

allows scientists and engineers to reliably probe physics in nanodevices which often produces signals too weak to detect at single device level.

Low-dimensional photodetectors were widely reported to have extraordinarily high gain (up to 10^{10}) [12]–[16], meaning that weak light-semiconductor interactions can be amplified into strong electrical signals by many orders of magnitude. Logically, it would be a good strategy to probe device physics in low-dimensional devices by leveraging the strong photoresponses. However, the classical photogain theory is an implicit function of device parameters, which thus cannot be used for fitting the photoresponses and probing device physics [17], [18]. More importantly, it was derived on two misplaced assumptions as we found previously [19], as a result of which it was incorrectly believed that high gain can be attained for any photoconductive semiconductors as long as the minority recombination lifetime is much longer than the transit time. After these two misplaced assumptions were corrected, we found a photoconductor intrinsically has no gain, or a small gain less than the ratio of majority to minority mobility [19]. The photogain comes from the surface depletion region in which the built-in electric field will pump the photogenerated majority carriers into the conduction channel [20]. Based on this model, we recently established an explicit photogain theory that can fit and predict the photoresponses and gain of nanoscale photodetectors [20]–[22]. In this work, we managed to find a large number of important device parameters at single nanowire level by a single fitting of the explicit theory to the experimental photoresponses. The extracted device parameters include surface depletion region widths W_{dep}, doping concentrations N_A (or N_D), majority carrier mobilities μ_p (or μ_n), minority recombination lifetime τ_0 and surface recombination velocity V_{srv}. The extracted parameters were verified with independent Hall effect measurements and other experiments.

II. RESULTS AND DISCUSSION

The silicon nanowires were fabricated by patterning the device layer of silicon-on-insulator (SOI) wafers with electron beam lithography followed by reactive ion etching, as shown in the optical microscopic image in Fig.1(a). To create p-type and n-type silicon nanowires, the device layers were pre-doped with boron and phosphorus at different doping concentrations,
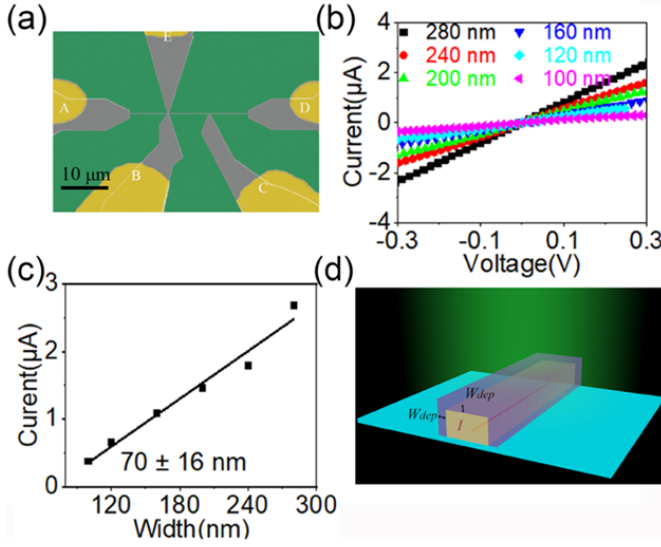
Fig. 1. (a) False color SEM image of a typical nanowire (200 nm wide). (b) I–V curves of p-type nanowires with different widths. (c) Current at a fixed bias for nanowires with different widths. (d) Diagram of nanowires with surface depletion regions under light illumination.
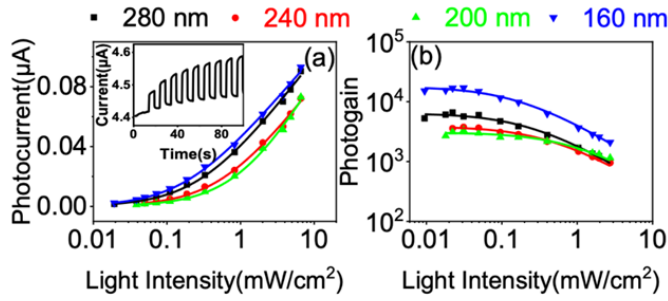
Fig. 2. Photoresponses of p-type nanowire photodetectors. (a) Photocurrent and (b) photogain of nanowire with different widths as a function of light intensity. Solid lines in (a) and (b) are the fitting curves following equations (1) and (2), respectively. Inset: transient current under the illumination of periodically modulated light.

respectively. All the nanowires are 27 μm long with a width varying from 100 nm to 300 nm. Five Si pads were made out of the device layer along with each nanowire for metal contacts during Hall effect and four-probe measurements. The fabrication details for nanowire devices can be found in our previous publication [21]. Fig.1(b) shows the current vs voltage (I-V) curves of p-type nanowires with different widths. At a fixed voltage, the current linearly decreases as the nanowires narrow down (Fig.1(c)), projecting to zero at a width of 70 ± 16 nm. It indicates that the nanowire has a surface depletion region width of 35 ± 8 nm. Considering that the device layer and the oxide underneath have a high-quality interface, the surface depletion region only exists in the nanowire side and top surfaces as shown in Fig.1d.

The current of a single nanowire under a fixed bias is modulated periodically by ON/OFF light illumination ($\lambda = 532$nm) with increasing intensity as shown in the inset of Fig. 2(a). The current base line increases slightly as the time goes by, likely because there exist slow trap states. The photocurrent is calculated from the difference between the ON and OFF current in each period. The photocurrent and photogain in

TABLE I
EXTRACTED PARAMETERS BY FITTING THE EQUATION (1)
TO THE EXPERIMENTAL DATA IN FIG. 2a

NW doping type	physical width W (nm)	P_{light}^s (mW/cm^2)	$\frac{\eta kT}{2qV_{bi0}}I_{ph}^s$ (nA)	W_{dep} (nm)	τ_0 (ns)	V_{srv} (10^4 cm/s)
p-type	280	0.31±0.03	28.1±1.0	28.0±1.2	0.54±0.02	1.55±0.05
	240	0.60±0.03	28.4±1.0	35.0±1.5	0.20±0.05	3.74±0.09
	200	1.19±0.03	37.8±1.0	42.5±1.5	0.12±0.00	5.75±0.07
	160	0.19±0.03	25.3±1.0	33.2±1.7	0.37±0.03	1.54±0.12
n-type	300	0.14±0.01	39.0±1.2	28.5±1.0	1.01±0.04	86.4±3.4
	260	0.03±0.01	30.1±1.6	24.6±0.8	5.42±1.47	14.8±1.4
	240	0.06±0.02	25.3±3.3	20.1±1.5	2.09±0.51	36.5±7.2
	220	0.02±0.03	18.2±0.5	18.4±2.9	4.77±0.41	15.1±0.8
	200	0.03±0.03	30.1±1.0	23.2±0.6	1.93±0.25	13.9±0.8

quantum efficiency for four different nanowires are plotted as a function of light intensity in Fig. 2(a) and (b), respectively.

Previously, we derived the analytical equations [21] for the photocurrent and photogain as shown in the equation (1) and (2) which fit well with the experimental data in Fig. 2(a) and (b), respectively. As the light intensity decreases, the photocurrent also decreases whereas the photogain reaches to its maximum value. The calibration error in weak light intensity and small photocurrent will create a large uncertainty in photogain. For this reason, we extracted the device physical parameters by fitting the photocurrent equation (1) to the experimental data in Fig. 2(a) instead of the photogain equation (2) to Fig.2(b).

$$I_{ph} = \frac{\eta kT}{2qV_{bi0}}I_{ph}^s ln\left(\frac{P_{light}}{P_{light}^s} + 1\right) \tag{1}$$

$$G = G_{max}\frac{P_{light}^s}{P_{light}}ln\left(\frac{P_{light}}{P_{light}^s} + 1\right) \tag{2}$$

In the above two equations, η is the ideality factor of surface depletion region as a Schottky junction, q is the unit of charge, V_{bi0} is the surface potential in the dark, G_{max} is the maximum photo gain at zero light intensity which is expressed as $G_{max} = \frac{\eta\hbar\omega kT I_{ph}^s}{2q^2V_{bi0}A_{proj}P_{light}^s}$ in which $\hbar\omega$ is the photon energy, kT is the thermal energy and A_{proj} is the nanowire area projected in the light incident direction. I_{ph}^s and P_{light}^s can be found in the equation (3) and (4) below.

$$P_{light}^s = \frac{\hbar\omega H n_i}{2\alpha\tau_0} \tag{3}$$

$$I_{ph}^s = q\mu_p p E_{ch} W_{dep}(2H_{ch} + W_{ch}), \tag{4}$$

in which μ_p is the majority carrier mobility, p the majority carrier concentration (also doping concentration N_A), E_{ch} the electric field intensity in the channel along nanowire axis, W_{dep} the surface depletion region width; H_{ch} the channel height, W_{ch} the channel width, H the nanowire physical height, n_i the intrinsic electron conentration of intrinsic silicon, α the light absorption ratio and τ_0 the effective minority recombination lifetime in the device. The light absorption ratio α can be found by finite differential time domain (FDTD) simulations.

When fitting equation (1) to the experimental data in Fig. 2(a), we extrated P_{light}^s and $\frac{\eta kT}{2qV_{bi0}}I_{ph}^s$ in Table I.

From P_{light}^s given by equation (3), we can find the effective minority recombination life time τ_0 listed in Table I. The estimated effective minority carrier lifetimes τ_0 are around sub-ns and a few ns for p-type and n-type nanowires, respectively, which are much shorter than those in bulk silicon due to strong surface recombination. Similarly short minority carrier lifetimes were also reported for nanowires in literature [23]. For a nanowire device with a rectangular cross-section, the effective minority carrier lifetime τ_0 is correlated with the surface recombination velocity V_{srv} by the equation (5). The term in the bracket on the right side of equation (5) is the surface-to-volume ratio in which the numerate for the height denominator is 1 instead of 2 because we assume that the surface recombination velocity is zero at the bottom surface (the high-quality interface of device layer and underneath oxide). From equation (5), the surface recombination velocity at the top and side surfaces can be caculated as shown in Table I.

$$\frac{1}{\tau_0} = \frac{1}{\tau_b} + (\frac{2}{W} + \frac{1}{H})V_{srv}, \tag{5}$$

in which τ_b is the minority recombination lifetime in bulk semiconductor which is at a scale of micro seconds, W is the nanowire width and H is the nanowire thickness.

The term $\frac{\eta kT}{2qV_{bi0}}I_{ph}^s$ with I_{ph}^s given by equation (4) has four unknown coupled parameters η, W_{dep}, μ_p and p. According to the semiconductor device principles, the ideality factor η is normally close to 2 as the surface recombination of nanoscale devices is the dominant recombination and generation paths in the surface depletion region. The other three unknown parameters can be found with two additional independent correlations in the following. The first correlation is the dark current or conductance of the device governed by the equation (6) in which the nanowire channel size H_{ch} and W_{ch} are unknown unless W_{dep} is provided. The second is the dependence of mobility on doping concentration given by the empirical Caughey-Thomas model in the equation (7).

$$I_{dark} = q\mu_p p E_{ch} H_{ch} W_{ch}, \tag{6}$$

where H_{ch} is the thickness of the nanowire channel ($=H\text{-}W_{dep}$); W_{ch} is the width of the nanowire channel ($=W\text{-}W_{dep}$).

$$\mu_p = \mu_{min} + \frac{\mu_{max} - \mu_{min}}{1 + (p/N_r)^{\alpha_1}} \tag{7}$$

For p-type Si, $\mu_{min} = 47.7$ cm^2 V^{-1}s^{-1}, $\mu_{max} = 495$ cm^2 V^{-1}s^{-1}, $\alpha_1 = 0.76$, $N_r = 6.3 \times 10^{16}$ cm^{-3}. For n-type Si, $\mu_{min} = 65$ cm^2 V^{-1}s^{-1}, $\mu_{max} = 1330$ cm^2 V^{-1}s^{-1}, $\alpha_1 = 0.72$, $N_r = 8.5 \times 10^{16}$ cm^{-3}.

Our previous work showed that the carrier mobilities in the nanowires remain the same as those in bulk silicon [21]. This experimental observation is consistent with the theoretical works in which surface scatterings will not be a dominant factor in carrier transport unless the nanowire diameter is less than 4 nm [24]–[26]. For this reason, equation (7) is still accurate enough for most nanowire devices reported in literature [12], [13], [22]. However, all nanoscale semiconductor devices synthesized by chemical vapor deposition
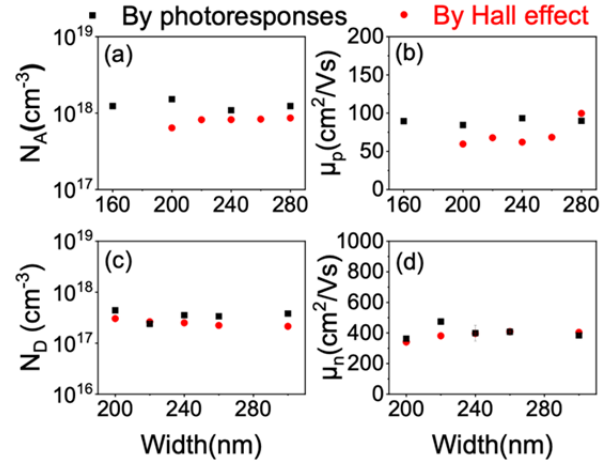
Fig. 3. Doping concentration and majority carrier mobility found from Hall measurements and photoresponse fittings for silicon nanowires. (a) and (b) p-type nanowires. (c) and (d) n-type nanowires.

have surface depletion regions which unfortunately were often neglected in the past. This negligence results in the conclusion that the mobilities decrease as nanowires reduce in diameter [4], [27], [28], which was incorrectly believed to be caused by surface scatterings.

The surface depletion region widths W_{dep} are found to be ~ 35 nm by calculation as shown in Table I, which is consistent with what we found independently from Fig.1(c). The calculated doping concentration N_A and majority carrier mobility μ_p are plotted as black squares in Fig. 3(a) and (b), respectively. To verify the doping concentration and carrier mobility, we performed Hall effect measurements at single nanowire level. The details of Hall measurements can be found in our previous publications [20], [21]. The measured doping concentrations and carrier mobilities are plotted as red dots in Fig. 3(a) and (b), respectively. The doping concentrations and mobilities found from Hall measurements are close to those extracted from photoresponses. We also repeated the measurements on n-type silicon nanowires in Fig. 3(c) and (d). Clearly, these device parameters, often difficult to calibrate at single device level, can be reliably found by fitting the photoresponses with our newly established analytical photogain theory.

III. Conclusion

In this work, we demonstrated a powerful tool to reliably extract many important device parameters by fitting the photoresponses with our newly established explicit photogain theory. This technique is can be readily applied to devices based on single-crystalline nanowires and thin films as long as there are surface depletion regions which can be created by surface states or by intentional surface doping to form a floating PN junction when the device surfaces are well passivation.

REFERENCES

[1] R.-S. Chen, T.-H. Yang, H.-Y. Chen, L.-C. Chen, K.-H. Chen, Y.-J. Yang, C.-H. Su, and C.-R. Lin, "High-gain photoconductivity in semiconducting InN nanowires," *Appl. Phys. Lett.*, vol. 95, no. 16, Oct. 2009, Art. no. 162112, doi: 10.1063/1.3242023.

[2] J. S. Jie, W. J. Zhang, Y. Jiang, X. M. Meng, Y. Q. Li, and S. T. Lee, "Photoconductive characteristics of single-crystal CdS nanoribbons," *Nano Lett.*, vol. 6, no. 9, pp. 1887–1892, Sep. 2006, doi: 10.1021/nl060867g.

[3] C. Soci, A. Zhang, X. Y. Bao, H. Kim, Y. Lo, and D. Wang, "Nanowire photodetectors," *J. Nanosci. Nanotechnol.*, vol. 10, no. 3, pp. 1430–1449, Mar. 2010, doi: 10.1166/jnn.2010.2157.

[4] A. C. Ford, J. C. Ho, Y.-L. Chueh, Y.-C. Tseng, Z. Fan, J. Guo, J. Bokor, and A. Javey, "Diameter-dependent electron mobility of InAs nanowires," *Nano Lett.*, vol. 9, no. 1, pp. 360–365, 2009, doi: 10.1021/nl803154m.

[5] X. Zhao and Y. Dan, "A silicon nanowire heater and thermometer," *Appl. Phys. Lett.*, vol. 111, no. 4, Jul. 2017, Art. no. 043504, doi: 10.1063/1.4985632.

[6] S.-K. Kim, K.-D. Song, T. J. Kempa, R. W. Day, C. M. Lieber, and H.-G. Park, "Design of nanowire optical cavities as efficient photon absorbers," *ACS Nano*, vol. 8, no. 4, pp. 3707–3714, Apr. 2014, doi: 10.1021/nn5003776.

[7] X. Gao, B. Guan, A. Mesli, K. Chen, and Y. Dan, "Deep level transient spectroscopic investigation of phosphorus-doped silicon by self-assembled molecular monolayers," *Nature Commun.*, vol. 9, no. 1, p. 118, Jan. 2018, doi: 10.1038/s41467-017-02564-3.

[8] D. V. Lang, "Deep-level transient spectroscopy: A new method to characterize traps in semiconductors," *J. Appl. Phys.*, vol. 45, no. 7, pp. 3023–3032, Jul. 1974, doi: 10.1063/1.1663719.

[9] W. Götz, G. Pensl, and W. Zulehner, "Observation of five additional thermal donor species TD_{12} to TD_{16} and of regrowth of thermal donors at initial stages of the new oxygen donor formation in czochralski-grown silicon," *Phys. Rev. B, Condens. Matter*, vol. 46, no. 7, pp. 4312–4315, Aug. 1992, doi: 10.1103/physrevb.46.4312.

[10] A. L. Endros, W. Kruhler, and F. Koch, "Electronic properties of the hydrogen-carbon complex in crystalline silicon," *J. Appl. Phys.*, vol. 72, no. 6, pp. 2264–2271, Sep. 1992, doi: 10.1063/1.351620.

[11] M. T. Asom, J. L. Benton, R. Sauer, and L. C. Kimerling, "Interstitial defect reactions in silicon," *Appl. Phys. Lett.*, vol. 51, no. 4, pp. 256–258, Jul. 1987, doi: 10.1063/1.98464.

[12] C.-J. Kim, H.-S. Lee, Y.-J. Cho, K. Kang, and M.-H. Jo, "Diameter-dependent internal gain in ohmic Ge nanowire photodetectors," *Nano Lett.*, vol. 10, no. 6, pp. 2043–2048, Jun. 2010, doi: 10.1021/nl100136b.

[13] C. Soci, A. Zhang, B. Xiang, S. A. Dayeh, D. P. R. Aplin, J. Park, X. Y. Bao, Y. H. Lo, and D. Wang, "ZnO nanowire UV photodetectors with high internal gain," *Nano Lett.*, vol. 7, no. 4, pp. 1003–1009, 2007, doi: 10.1021/nl070111x.

[14] R. H. Bube, *Photoelectronic Properties of Semiconductors*. Cambridge, U.K.: Cambridge Univ. Press, 1992.

[15] A. Rose, *Concepts in Photoconductivity and Allied Problems*, no. 19. Brussels, Belgium: Interscience Publishers, 1963.

[16] G. Konstantatos, M. Badioli, L. Gaudreau, J. Osmond, M. Bernechea, F. P. G. de Arquer, F. Gatti, and F. H. L. Koppens, "Hybrid graphene-quantum dot phototransistors with ultrahigh gain," *Nature Nanotechnol.*, vol. 7, pp. 363–368, Jun. 2012, doi: 10.1038/nnano.2012.60.

[17] R. L. Petritz, "Theory of photoconductivity in semiconductor films," *Phys. Rev.*, vol. 104, no. 6, pp. 1508–1516, Dec. 1956, doi: 10.1103/PhysRev.104.1508.

[18] D. A. Neamen, *Semiconductor Physics and Devices: Basic Principles*, 4th ed. New York, NY, USA: McGraw-Hill, 2011.

[19] Y. Dan, X. Zhao, K. Chen, and A. Mesli, "A photoconductor intrinsically has, no gain," *ACS Photon.*, vol. 5, no. 10, pp. 4111–4116, Oct. 2018, doi: 10.1021/acsphotonics.8b00805.

[20] K. Chen, X. Zhao, A. Mesli, Y. He, and Y. Dan, "Dynamics of charge carriers in silicon nanowire photoconductors revealed by photo Hall effect measurements," *ACS Nano*, vol. 12, no. 4, pp. 3436–3441, Apr. 2018, doi: 10.1021/acsnano.8b00004.

[21] J. He, K. Chen, C. Huang, X. Wang, Y. He, and Y. Dan, "Explicit gain equations for single crystalline photoconductors," *ACS Nano*, vol. 14, no. 3, pp. 3405–3413, Mar. 2020, doi: 10.1021/acsnano.9b09406.

[22] J. He, H. Liu, C. Huang, Y. Jia, K. Li, A. Mesli, R. Yang, Y. He, and Y. Dan, "Analytical transient responses and gain–bandwidth products of low-dimensional high-gain photodetectors," *ACS Nano*, vol. 15, no. 12, pp. 20242–20252, Dec. 2021, doi: 10.1021/acsnano.1c08331.

[23] Y. P. Dan, K. Seo, K. Takei, J. H. Meza, A. Javey, and K. B. Crozier, "Dramatic reduction of surface recombination by *in situ* surface passivation of silicon nanowires," *Nano Lett.*, vol. 11, no. 6, pp. 2527–2532, Jun. 2011, doi: 10.1021/nl201179n.

[24] M. T. Björk, H. Schmid, J. Knoch, H. Riel, and W. Riess, "Donor deactivation in silicon nanostructures," *Nature Nanotechnol.*, vol. 4, no. 2, pp. 103–107, 2009, doi: 10.1038/nnano.2008.400.

[25] E. B. Ramayya, D. Vasileska, S. M. Goodnick, and I. Knezevic, "Electron transport in silicon nanowires: The role of acoustic phonon confinement and surface roughness scattering," *J. Appl. Phys.*, vol. 104, no. 6, Sep. 2008, Art. no. 063711, doi: 10.1063/1.2977758.

[26] S. Jin, M. V. Fischetti, and T.-W. Tang, "Modeling of electron mobility in gated silicon nanowires at room temperature: Surface roughness scattering, dielectric screening, and band nonparabolicity," *J. Appl. Phys.*, vol. 102, no. 8, Oct. 2007, Art. no. 083715, doi: 10.1063/1.2802586.

[27] Z. X. Yang, S. Yip, D. Li, N. Han, G. Dong, X. Liang, L. Shu, T. F. Hung, X. Mo, and J. C. Ho, "Approaching the hole mobility limit of GaSb nanowires," *ACS Nano*, vol. 9, no. 9, pp. 9268–9275, Sep. 2015, doi: 10.1021/acanano.5b04152.

[28] S. H. Lee, T. I. Lee, S. J. Lee, S. M. Lee, I. Yun, and J. M. Myoung, "Electrical characteristics of metal catalyst-assisted etched rough silicon nanowire depending on the diameter size," *ACS Appl. Mater. Interface*, vol. 7, no. 1, pp. 929–934, Jan. 2015, doi: 10.1021/am507478q.